Spectra of dark and bright excitons in alloyed nanowire quantum dots

M. Zieliński*

Institute of Physics, Faculty of Physics, Astronomy and Informatics, Nicolaus Copernicus University, Grudziadzka 5, 87-100 Torun, Poland

(Received 10 October 2018; revised manuscript received 22 May 2019; published 24 July 2019)

Excitons in alloyed nanowire quantum dots exhibit unique spectra, as shown here using atomistic calculations. The bright exciton splitting is triggered solely by alloying, despite the cylindrical quantum dot shape reaching over 15 μeV. These results are contrary to previous theoretical predictions; however, they are in line with experimental data. This splitting can nonetheless be tuned by an electric field to go below the 1 μeV threshold. The dark exciton optical activity is also strongly affected by alloying that reaches a notable 1/3500 fraction of the bright exciton and has a large out-of-plane polarized component.

DOI: 10.1103/PhysRevB.100.045309

I. INTRODUCTION

The main spectral properties of quantum dots [1] (QDs) are governed by their size, shape, and average chemical composition [2,3]. However, the detailed, fine structure of their optical spectra [4], which plays an essential role for their applications in quantum optics [5–7] and information [8–10], is determined by atomic-scale details related to the microscopic symmetry of the underlying lattice [11–14], the presence of facets [15], and the alloying randomness [16–19]. Regarding potential applications, the bright exciton (BE) recombination in QDs is considered to be a tool for the generation of entangled photons through biexciton-exciton cascades [20,21]. In contrast, the dark exciton (DE) gained attention as a candidate for long-lived, although optically addressable, quantum bits [15,22–26]. The DE is also considered an auxiliary state for time-bin entanglement generation schemes [27–29].

In self-assembled quantum dots (SADs), the efficiency of entanglement generation is limited by the distortions [4,17] of the QD confining potential from an idealized cylindrical symmetry [11,30–32]. The overall low symmetry [11,30–32] induces splitting of optically active excitonic lines, that is, bright exciton splitting (BES), also known as fine-structure splitting [4]; this prohibits entanglement generation. As controlling the shape of SADs is restricted by the character of epitaxial growth, several postgrowth methods [33–35] have been developed that aim to reduce BES, in particular by the utilization of external fields [7,36–45]. Further research also focused on the growth itself by using the ripening [46] process, droplet epitaxy for low-strain QDs [47], or vapor-liquid-solid (VLS) growth of nanowire QDs (NWQDs) [48–53]. The general concept is to restore high symmetry of a QD in order to reduce its fine-structure splitting. This is particularly based on theoretical predictions [11,31,32] indicating that the triangular (C_{3v}) symmetry of a nanostructure will lead to the vanishing BES. Moreover, in the case of VLS-grown NWQDs the empirical pseudopotential method (EPM) predicts vanishing BES for both pure (C_{3v}) and alloyed (C_1) NWQDs [11]. However, measurements [54,55] of fine-structure splitting in alloyed NWQDs show clear disagreement between the experimental results and the results of the theoretical EPM. Notably, the EPM predicts [11] a nearly vanishing fine structure (0.2 μeV) even in heavily alloyed $InAs_{0.25}P_{0.75}$ NWQDs, whereas experiments [54,55] reveal BES for alloyed NWQDs varying in a broad range of values and reaching up to 16–18 μeV. In the case of VLS lithography and NWQDs, alloying is unavoidable and originates from the presence of the eutectic growth seed [56]. This leads to a pronounced, up to 80% [52,57], intermixing of the barrier (InP) material into the (InAs) QD region, effectively producing heavily alloyed (e.g., $InAs_{0.2}P_{0.8}$) NWQDs. In order to achieve the entanglement of emitted photon pairs in alloyed NWQDs, researchers thus must conduct a postgrowth [54] search of low-BES samples, somewhat similar to SADs [35] and in clear contradiction to the results of the EPM.

The disagreement between the BES results of the EPM and those of experiments can be observed not only for NWQDs but also for various QD systems [16]. This is generally a puzzle, as the EPM is an atomistic approach. The users and developers of this method, in fact, have acknowledged this disagreement [16]: "It seems that the variations in shape, size, or composition, we can assume theoretically, are not able to bring theory and experiment in agreement." The authors of Ref. [16], however, suggest that other effects such as "ordering" are responsible for this disagreement between the theoretical and experimental results rather than the method itself. This explanation, however, does not necessarily apply to NWQDs, and further research on the subject is required.

In this work, by atomistic, empirical tight-binding calculations, the fundamental role of composition disorder in NWQDs is shown. In particular, a pronounced BES reaching over 15 μeV stemming entirely from alloy randomness, with no QD shape elongation [19,58,59] or compositional inhomogeneity, is shown [55]. The results are in good agreement with the experimental results, yet they contradict EPM predictions. Further, an efficient BES reduction scheme in NWQDs is proposed via an externally applied vertical electric field. Compared to SADs, NWQDs show a very different, Gaussian-like dependence without a lower bound [17,37,41]. Contrarily,

*mzielin@fizyka.umk.pl

 ©2019 American Physical Society

the DE splitting in alloyed NWQDs practically vanishes (below 0.3 μeV) despite the mixed chemical composition and alloying. The strength of the DE oscillator is significantly increased by alloying and changes in the QD height, reaching a notable 1/3500 fraction of the BE without any NWQD shape alteration [15,60]. The DE polarization properties are also strongly affected by alloying. In case of nonalloyed or weakly alloyed systems the DE emission is polarized in plane (x/y), whereas in the case of strongly alloyed NWQDs, this emission gains a strong, even dominant, out-of-plane (z) component.

II. METHODS

The calculations are performed in a series of computational steps beginning with the valence force field [61–64] approach for strain, empirical tight binding [65–69] for single-particle spectra, and configuration interaction for many-body excitonic properties [70–74].

In the first calculation step, in order to account for the lattice mismatch between InAs QDs and InP nanowires, the strain-relaxed positions are calculated using the atomistic valence force field approach of Keating [61] with the minimization of the strain energy performed using the conjugate gradient method [67]. Systems modeled in this work are known as capped or cladded [51] nanowire QDs, where the host nanowire diameter (reaching 100 nm in the experiment) is much larger than that of QDs. Therefore, the boundary condition for strain calculations is used assuming the InP bulk lattice is constant on the nanowire surface. The valence force field (VFF) method is described in more detail in Refs. [63,64] and in previous papers [67–69,71].

The atomic positions determined from strain calculations are used to determine single-particle energies with the empirical nearest-neighbor tight-binding model that accounts for strain, spin-orbit interactions, and d orbitals. [68,69] The single-particle tight-binding Hamiltonian for the system of N atoms and m orbitals per atom can be written, in the language of the second quantization, in the following form:

$$\hat{H}_{\mathrm{TB}} = \sum_{i=1}^{N}\sum_{\alpha=1}^{m} E_{i\alpha} c_{i\alpha}^{+} c_{i\alpha} + \sum_{i=1}^{N}\sum_{\alpha=1,\beta=1}^{m} \lambda_{i\alpha,\beta} c_{i\alpha}^{+} c_{i\beta} + \sum_{i=1}^{N}\sum_{j=1}^{\text{near.neigh.}}\sum_{\alpha,\beta=1}^{m} t_{i\alpha,j\beta} c_{i\alpha}^{+} c_{j\beta}, \quad (1)$$

where $c_{i\alpha}^{+}$ $(c_{i\alpha})$ is the creation (annihilation) operator of a carrier on the (spin-)orbital α localized on site i, $E_{i\alpha}$ is the corresponding on-site (diagonal) energy, and $t_{i\alpha,j\beta}$ describes the hopping (off site, off diagonal) of the particle between the orbitals on (four) nearest-neighbor sites. The summation i goes over all atoms, whereas the summation over j goes over only the four nearest neighbors. α is a composite (spin and orbital) index of an on-site orbital, whereas β is a composite index of a neighboring atom orbital. Coupling to further neighbors is thus neglected, while $\lambda_{i\alpha,\beta}$ (on site, off diagonal) accounts for the spin-orbit interaction following the description given by Chadi [75] and includes only the contributions from the atomic p orbitals.

The tight-binding parameter set from Ref. [66] is used for $sp^3d^5s^\star$ parametrization. This parametrization utilizes one s, three p, five d, and one excited s^* orbitals for each site and each spin component, leading to (with spin) a total of 20 [$m = 20$ in Eq. (1)] spin-orbitals per atom. Dangling bonds are passivated on the surface to exclude nonphysical (spurious) states. The passivation is modeled by shifting the energy of these bonds high above the conduction band edge such that they do not modify states near the band gap [76]. As this work aims to model QDs well embedded inside nanowires and separated from the surface by a thick cladding, the effects owing to image charge buildup in a nanowire surface are neglected.

The tight-binding computations are performed on a smaller domain (subsection of nanowire) than that used in the VFF calculation [76,77]. The number of atoms in the tight-binding simulation is equal to ≈0.7 million, whereas the number of atoms in the VFF simulation reaches over 18 million atoms. The length of nanowire section used in the VFF simulation is equal to ≈120 nm (with 72-nm diameter). The section of nanowire (including the quantum dot and surrounding nanowire material) used for the TB calculation has an ≈36-nm diameter and is ≈18 nm long.

These dimensions guarantee the convergence of single-particle spectra well below 1 meV [76,77]. More details of the $sp^3d^5s^\star$ tight-binding calculation were provided in our earlier papers [67–69,71,74].

Finally, the single-particle calculation is followed by a many-body calculation to obtain excitonic spectra and, in particular, the excitonic fine structure. The Hamiltonian for the interacting electrons and holes can be written in the second quantization [2] and, in particular for the single exciton, is given as [71,74]

$$\hat{H}_{ex} = \sum_i E_i^e c_i^\dagger c_i + \sum_i E_i^h h_i^\dagger h_i - \sum_{ijkl} V_{ijkl}^{eh,\mathrm{dir}} c_i^\dagger h_j^\dagger h_k c_l + \sum_{ijkl} V_{ijkl}^{eh,\mathrm{exchg}} c_i^\dagger h_j^\dagger c_k h_l, \quad (2)$$

where E_i^e and E_i^h are the single-particle electron and hole energies, obtained at the single-particle stage of calculations, respectively, and V_{ijkl} are Coulomb matrix elements [71,72]. The many-body Hamiltonian for the exciton is solved using the configuration interaction (CI) approach [70,71], where the Coulomb matrix elements (Coulomb direct and exchange integrals) are calculated according to the procedure given in Ref. [71]. The CI approach involves an electron-hole configuration built from the lowest six (with spin, 12) electron states and six (with spin, 12) hole states. This approach thus effectively accounts for s, p, and d electron and hole QD shells [1].

III. PHOSPHOROUS CONTENT AND ALLOYING

Figure 1 shows results obtained for an alloyed NWQD as a function of phosphorus content. The QD is disk shaped with a diameter of 30 nm and a height of 4.2 nm; it is embedded in a [111]-oriented InP host zinc-blend nanowire with a diameter of 72 nm. To account for alloying, a uniform composition profile is used that mimics the migration of P anions into the

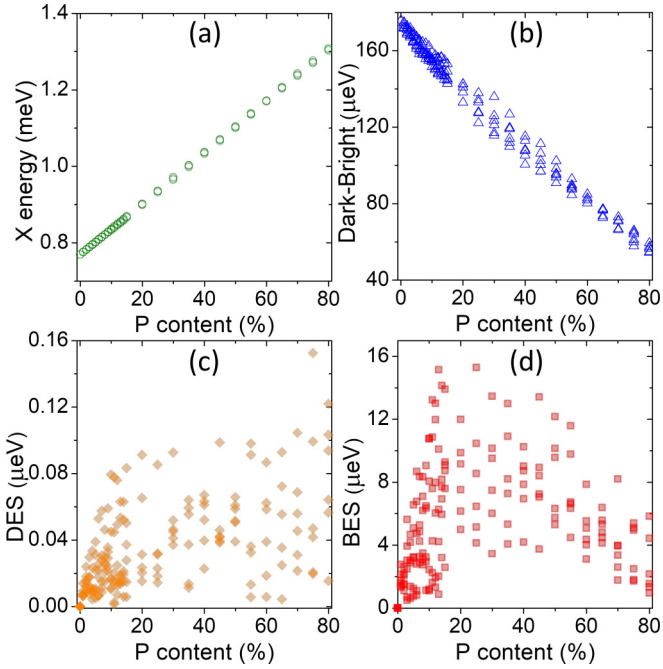

FIG. 1. (a) Exciton ground-state energy, (b) dark-bright exciton splitting and (c) dark and (d) bright exciton splitting as a function of phosphorous content in the alloyed NWQD.

QD during VLS growth. The overall nanostructure's symmetry is C_{3v} for pure InAs systems and is reduced by alloying to C_1. At each P content, there are six randomly generated samples corresponding to the same average composition [18]. The P content is varied from 10% to 80% with a 5% increment and from 0% to 10% with a 1% increment for greater accuracy. Thus, there are 29 various average compositions with 6 random samples per composition, totaling 174 different nanostructures and presenting a challenging computational problem.

In Fig. 1(a) the ground excitonic energy increases with P content, from 768 meV for pure InAs to approximately 1305 meV for $InAs_{0.2}P_{0.80}$ QDs. This increase in the excitonic energy is caused by the introduction of a higher band gap energy barrier material into the QD; further, it is linear to a good approximation with a 6.7 meV/% slope. The spread of excitonic energies owing to alloy randomness reaches almost 8 meV and is practically nonapparent in Fig. 1(a). In contrast, the dark-bright splitting [Fig. 1(b)], i.e., the energy difference between the lowest BE and the higher-energy DE, reduces with an increase in P content as the P admixture effectively decreases the depth of confinement and thus the so-called isotropic [4] electron-hole exchange, which controls the dark-bright splitting. The spread of calculated values is notable, with a maximum value of approximately 20 μeV for a P content of 30%; it then decreases with P. Intuitively, this can be understood in terms of a number of different possible phosphorous atomic arrangements (combinations), increasing with P, reaching a maximum at P = 50%, and then reducing again. Speculatively, this effect combined with the overall decrease in dark-bright splitting owing to increasing P content (shallower confinement) leads to a maximal spread at P $\approx$ 30% rather than P = 50%.

The impact of alloy randomness on excitonic fine structure [Figs. 1(c) and 1(d)] is fundamentally stronger. Both the dark exciton splitting (DES) and BES are exactly zero by symmetry for pure InAs NWQDs; however, a small percentage of P admixture introduces non-negligible splittings. For the BES [Fig. 1(d)], these splittings reach maximal values of about 15 μeV for a P content between 10% and 30%, and interestingly, these maxima are quenched again with further alloying, arguably owing to the same mechanism as for the dark-bright splitting.

Alloy randomness by itself increases with P, reaches a maximum at $P = 50\%$, and then decreases. Therefore, if alloy randomness would be the only factor affecting the BES, then its distribution in Fig. 1(d) should be symmetrical with respect to the P content. However, as observed earlier, with an increasing P content, there is also a reduction in the confining potential depth and therefore, a reduction in the overall strength of the electron-hole Coulomb and exchange interaction. Namely, for $P = 0\%$ (or $As = 100\%$), the confinement is the strongest, whereas for $P = 100\%$ ($As = 100\%$), there is no confinement at all. This latter case would actually correspond to an empty InP nanowire without a QD.

Thus, the overall trend of the BES evolution as a function of P appears to be a convolution of alloy randomness (that has a maximum at P = 50% and is symmetrical with respect to P or As content) and quasilinear reduction in confinement (and thus the magnitude of Coulomb and exchange integrals) that decreases with P content. Finally, this leads to a BES maximum around P = 20% or P = 30% rather than one at P = 50% [Fig. 1(d)].

For P content between 20% and 60%, minimal values of BES do not drop below approximately 3 μeV. Only for the lowest P concentrations and for P contents over 70% does the BES drop below 1 μeV. Apart from being typically much greater than EPM predictions [11], these values also show pronounced dot-to-dot fluctuations as seen in the experiment [54]. Similarly, the DES [Fig. 1(c)] is also triggered by alloying; however, this splitting is very small, often below 0.11 μeV. Maximal values of the DES increase with P up to about P = 20%. Then, the trend saturates with only some spikes (of approximately 0.15 μeV) for the largest considered P of 75%–80%. The DES distribution is more uniform with no apparent lower bound.

To understand the significant differences between magnitudes of DES and BES owing to alloying, exchange integrals which are predominately (i.e., when neglecting configuration mixing with higher levels) responsible for the presence of these splittings are examined. Using the standard notation [4,78], the exchange integral mixing two bright excitonic configurations, with antiparallel $\uparrow\Downarrow$, $\downarrow\Uparrow$ electron and hole quasispins, which leads to BES, is given as [4,69]

$$\begin{aligned} \mathrm{BES} &\approx 2\langle\uparrow\Downarrow|1/\epsilon|\boldsymbol{r_1}-\boldsymbol{r_2}||\downarrow\Uparrow\rangle \\ &= 2\iint \frac{e^*_\uparrow(\boldsymbol{r_1})h^*_\Downarrow(\boldsymbol{r_2})e_\downarrow(\boldsymbol{r_2})h_\Uparrow(\boldsymbol{r_1})d\boldsymbol{r_1}d\boldsymbol{r_2}}{\epsilon|\boldsymbol{r_1}-\boldsymbol{r_2}|}, \end{aligned} \tag{3}$$

where e and h are the electron and the hole ground states, respectively, with arrows representing their quasispins. ϵ is the dielectric screening [71]. A factor of 2 is included as the splitting magnitude is twice the value of the integral [4].

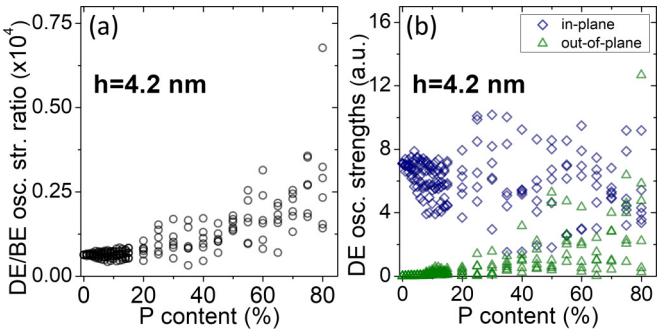

FIG. 2. (a) Ratio of dark to bright exciton oscillator strengths and (b) dark exciton polarization properties as a function of phosphorous content in the alloyed NWQDs. Blue diamonds and green triangles denote in-plane and out-of-plane polarizations, respectively.

Similarly, the DE mixing term and the corresponding splitting magnitude are given as

$$\mathrm{DES} \approx 2\langle\uparrow\Uparrow|1/\epsilon|\boldsymbol{r_1}-\boldsymbol{r_2}||\downarrow\Downarrow\rangle = 2\iint \frac{e^*_\uparrow(\boldsymbol{r_1})h^*_\Uparrow(\boldsymbol{r_2})e_\downarrow(\boldsymbol{r_2})h_\Downarrow(\boldsymbol{r_1})d\boldsymbol{r_1}d\boldsymbol{r_2}}{\epsilon|\boldsymbol{r_1}-\boldsymbol{r_2}|}, \quad (4)$$

where parallel ($\uparrow\Uparrow$, $\downarrow\Downarrow$) quasispin alignments correspond to DE configurations. In cases of high C_{3v} symmetry, both of these (bright and dark) exchange integrals would vanish. Alloying breaks the symmetry, and the angular momentum is no longer a good quantum number. In such a situation, the single-particle states with arrows denote states in Kramers degenerate doublets [79,80] rather than pure angular momentum states, with $\uparrow$ being the electron state of predominately quasi-spin-up character, but with (some) small quasi-spin-down contribution, with similar notation for hole states. Thus, at a given point $\boldsymbol{r_1}$ (or $\boldsymbol{r_2}$), quasicharges with antiparallel quasispins (contributing to the DES) are expected to be much smaller than those with parallel quasispins; hence, the DES tends to be systematically much smaller than the BES.

A. Dark exciton optical activity

Alloying has a strong impact on oscillator strengths of excitons, particularly on the DE that gains a substantial optical activity, as shown in Fig. 2(a), where the ratio of the DE to BE oscillator strengths is used as a measure of relative DE optical activity. For idealized, high-symmetry C_{3v} QDs without alloying, the DE is expected to exhibit a very weak (yet nonvanishing) optical activity owing to symmetry-dependent selection rules [31,32]. More simplified effective mass approaches (neglecting the presence of a low-symmetry crystal lattice and assuming a cylindrical C_∞ symmetry) actually predict completely vanishing optical activity of DEs [4]; this is how its name originated. Alloying breaks the high symmetry and thus loosens selection rules (whether derived by group-theoretical or effective mass arguments), allowing the DE to gain some optical activity. Here, for a nonalloyed C_{3v} QD, the DE oscillator strengths are approximately 160 000 times weaker than the BE strengths. However, for the alloyed C_1 NWQDs, this activity is increased significantly up to an approximately 1/30 000 fraction of the BE [even up to 1/15 000 for one extreme case shown in Fig. 2(a)], with a further (by the factor of several) increase in taller QDs, as discussed later.

B. Dark and bright exciton polarizations

Alloying also affects the polarization properties of NWQDs. For the BE, the emitted light is (to a very good approximation) polarized in the QD plane, yet with in-plane linear polarization directions randomized from dot to dot. The randomization of BE polarization is similar and consistent with the theoretical predictions for alloyed self-assembled InGaAs QDs [81]. The BE emission is thus in plane polarized with a much weaker (6 orders of magnitude) out-of-plane (growth direction, z) component. For the disk-shaped NWQD, there is little BE polarization anisotropy, which increases with alloying and reaches approximately 1% at P = 0.8.

The DE optical spectra and polarization properties of alloyed systems are also interesting [Fig. 2(b)]. For the pure InAs C_{3v} NWQD, the DE is (as mentioned above) very weak, yet it is completely polarized in plane, having exactly the same polarization properties as the BE [32]. Such DE polarization properties are different from self-assembled C_{2v} QDs yet fully consistent with group-theoretical predictions for C_{3v} nanostructures [11,31,32]. However, with an increase in P content and a reduction in symmetry from C_{3v} to C_1, the DE gains a large out-of-plane component of the emission. For the highest considered P content, the out-of-plane oscillator strengths are comparable to and can even exceed the in-plane ones. This is different from low-symmetry InAs/GaAs SADs [15], where the dark-bright exciton mixing effects seem to dominate the spectra. This is also different from nonalloyed InAs/InP C_{3v} QDs [11,32], where, as mentioned above, the DE exactly follows the polarization of the BE and only has an in-plane component, i.e., the case of P = 0% in Fig. 2(b). In fact, the DE in alloyed (P $\neq$ 0%) NWQDs appears to have intermediate properties. "Lattice randomization" as induced by alloying makes out-of-plane DE exciton components comparable with in-plane ones, somewhat overcoming the effects of strong confinement (small quantum dot height) in the growth direction. Therefore, the DE (weak) optical activity and polarizations are strongly susceptible to local atomic arrangement in the underlying lattice. This is somewhat contrary to the BE polarizations, the properties of which are, to a large degree, determined by an overall quasi-two-dimensional confinement of a disk-shaped QD and alloying not being able to generate a significant out-of-plane BE polarized component, which practically vanishes. Alloying thus impacts the BE polarization by randomizing its in-plane directions, yet it has a more significant effect on the DE by allowing for its emission to be polarized in all three spatial directions. This effect is nontrivial and is discussed further in the following section.

IV. ROLE OF QUANTUM DOT HEIGHT

It is also interesting to investigate how spectra of excitons in alloyed NWQDs depend on the growth direction confinement. This is shown in Figs. 3 and 4, where the height of NWQDs varies from 1.4 to 8.4 nm (11 different cases). All other QD and nanowire dimensions are the same as described above. Four different P concentrations were considered

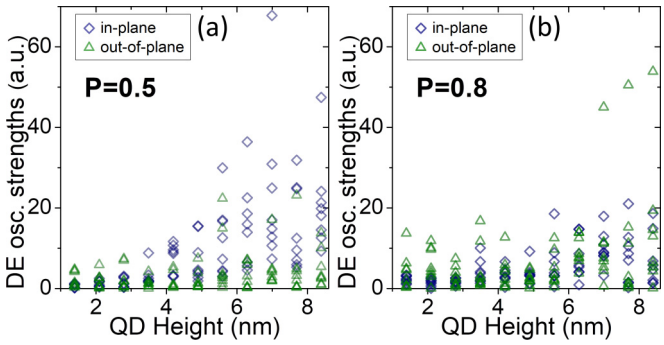

FIG. 3. Dark exciton polarization properties as a function of height for alloyed NWQDs and two average compositions, (a) $InAs_{0.5}P_{0.5}$ and (b) $InAs_{0.2}P_{0.8}$. Blue diamonds and green triangles denote in-plane and out-of-plane polarizations, respectively.

(P = 50% and 80%, as well as 60% and 70% for a comparison). There were eight random samples generated for each average composition, leading to a formidable problem of $(11 \times 4 \times 8)$ 352 separate atomistic computations.

A. Dark exciton polarizations

For $InAs_{0.5}P_{0.5}$ NWQDs and heights lower than 3 nm, the DE is mostly out of plane polarized with weak in-plane components [Fig. 3(a)]. This is very interesting, and it appears that owing to the randomness, the DE polarization properties in flat alloyed NWQDs resemble more closely C_{2v} SAD spectra [32], with DE z polarized emission, compared with C_{3v} pure InAs NWQDs with x/y polarization. In other words, strong lattice randomization, owing to 50% alloying, combined with strong confinement in the vertical direction (i.e., small quantum dot height) effectively diminishes ("smears") the role of nanowire/lattice symmetry. DE polarizations in such nanostructures mimic that of flat SADs, and they could be adequately modeled in terms of the effective mass approach [82]. However, with the increase in the QD height, the in-plane component grows faster than the out-of-plane one, and the in-plane polarization dominates the tall QD DE spectra for P = 0.5. Here, despite the alloying, the effect of the substrate (nanowire) orientation is apparently pronounced, and the polarization properties of the DEs are similar to those predicted for idealized C_{3v} systems.

For heavily alloyed P = 0.8 systems and small QD heights, the DE emission is mostly out of plane polarized [Fig. 3(a)], underlying the key role of the strong confinement (flat quantum dot) in the growth direction. However, for taller QDs (and high P = 0.8 content) both components of polarization are comparable. In fact, there are several notable cases where the out-of-plane polarization becomes dominant for $h > 7$ nm. This is very distinct from nonalloyed C_{3v} systems; in such systems alloying appears to dominate the DE spectra over the substrate/symmetry effects. Overall, the DE polarization properties vary from dot to dot and are pronounced and nontrivial functions of both confinement and alloying.

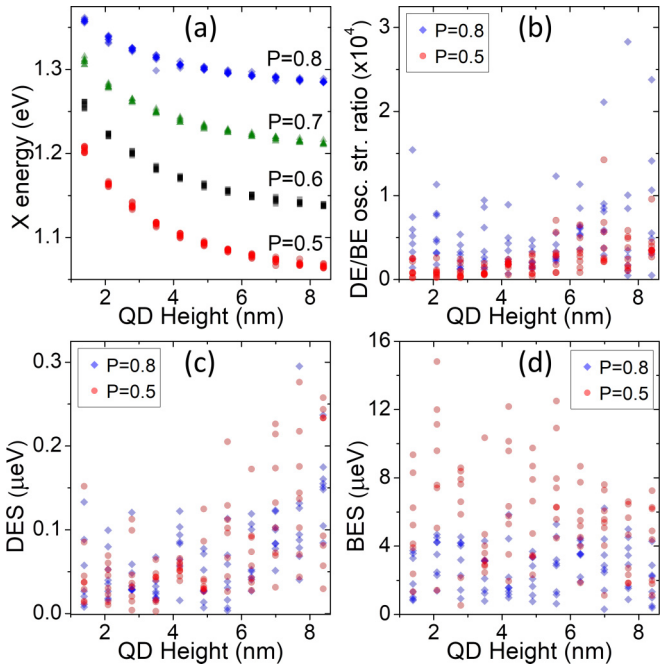

FIG. 4. (a) Exciton ground-state energy, (b) bright and (c) dark exciton splitting, and (d) dark to bright exciton oscillator strength ratio as a function of alloyed NWQD height; different symbols and colors denote phosphorous contents.

B. Fine-structure splittings

Further studies on the height dependence of QDs are shown in Fig. 4. Here, for completeness, Figure 4(a) presents the ground excitonic state energy evolution as a function of both the height and P content. The increased QD height reduces the confinement and decreases the excitonic energy, whereas the P content increases the excitonic energy and flattens the trends. The spread of the calculated values owing to alloy randomness is relatively small (≈10 meV). Figure 4(b) shows the DE activity with respect to BE, similar to Fig. 2(a), as a function of QD height. For P = 0.5, DE optical activity increases approximately fivefold as a result of the reduced confinement. Similarly, for P = 0.8, the ratio of the DE/BE oscillator strength is much larger for taller QDs than for the flat ones, with the exception of extremely flat, several monolayers (<2 nm) thick QDs, where the DE/BE ratio is also increasing. Notably, for highly alloyed and high-aspect-ratio tall QDs, the DE can achieve significant optical activity (for extreme cases) equal to a notable 1/3500 fraction of the BE. Finally, note that there is a pronounced dot-to-dot variation and a substantial spread of the DE optical activity owing to the alloy randomness between NWQDs of the same height and average composition.

Further, Figs. 4(c) and 4(d) present the DES and BES, respectively, as a function of QD height. The DES spread increases with QD height, reaching approximately 0.15 μeV for $h < 5$ nm and approximately 0.3 μeV for taller systems. Thus, the lower bound of the DE spin's coherent precession time [83] (Planck's constant divided by the eigenstates' energy difference) will typically exceed 14 ns, an important figure for potential DE applications [22]. For the DES, there is no apparent difference between P cases, which is in agreement with the earlier discussions. In contrast, the BES shows nearly no dependence on the QD height and a strong dependence on

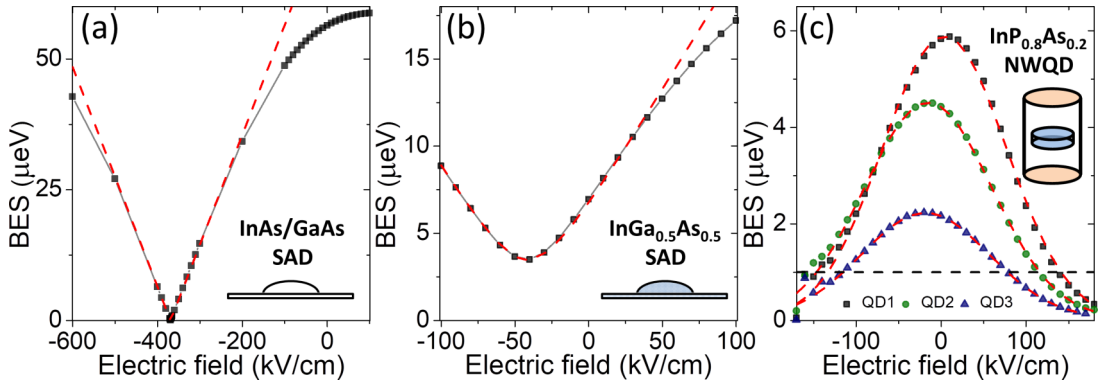

FIG. 5. Bright exciton splitting as a function of vertical electric field for (a) nonalloyed InAs/GaAs SAD, (b) alloyed $InGa_{0.5}As_{0.5}$/GaAs SAD, and (c) three different alloyed NWQDs with the same average composition $InP_{0.8}As_{0.2}$/InP.

the P content. For $P = 0.5$, the BES is generally 2 to 3 times larger than that for $P = 0.8$. Thus, the BES is reduced with a large alloying, which is in agreement with previous results. Notably, the BES varies considerably between the distinct QDs, and only a small group of QDs will have a BES below the conventional threshold of 1 μeV, which is consistent with experimental findings and in disagreement with the EPM predictions.

V. EXTERNAL ELECTRIC FIELD

The control of the BES with an external field is important for its applicability [21]. Figure 5 shows the effect of a vertical electric field [84] applied to NWQDs as well as SADs for comparison [37]. Two lens-shaped SADs are considered: a nonalloyed InAs of C_{2v} symmetry and alloyed $InGa_{0.5}As_{0.5}$ of C_1 symmetry. The SADs' dimensions are identical, with diameters of 25 nm and heights equal to 3.5 nm. Both SADs are embedded in a GaAs barrier and are placed on a two-monolayer-thick (0.6 nm) InAs wetting layer. As for the NWQDs, three different $InP_{0.8}As_{0.2}$ alloyed dots are shown in Fig. 5(c). These NWQDs have identical dimensions ($h =$ 4.2 nm, $d = 30$ nm) and average composition, the only difference between them being random alignment of P atoms. Separate empirical tight binding (ETB) and CI calculations were performed for a total of 215 different cases.

For the C_{2v} SAD the zero-field BES [Fig. 5(a)] is large and equal to 56.4 μeV. The field influences this splitting and can even reverse the order of BE lines [37]. Alloying reduces [34] BES in SADs, and for $InGa_{0.5}As_{0.5}$, the BES at zero field is approximately 7 μeV [Fig. 5(b)], whereas the field can reduce the BES to its lower bound [11,37] of 3.5 μeV. These results are in agreement with those from experiment for similar QDs [37]. Atomistic calculation can be well fit [85] [red dashed lines in Figs. 5(a) and 5(b)] to the phenomenological model proposed in Ref. [37].

In SADs, electric field tuning of the BES stems from a dipole moment along the growth direction [37,86] owing to the asymmetric shape of SADs [86]. In NWQDs, there is no shape asymmetry. There is an inversion asymmetry [12,87] related to the [111] growth that spatially shifts the electron and the hole [74]. This effect, however, does not trigger the BES, which is exactly zero for C_{3v}, and the BES is only due to alloying. Moreover, NWQDs show a peculiar field BES evolution [Fig. 5(c)]. A particle in the box model, assuming an infinite square well, relating the BES to the oscillator strength [58] and using perturbation theory up to second order, gives the BES dependence as follows: $s_0 - \alpha F^2 + \beta F^4$, where s_0 is the zero-field F splitting and α and β are constants. For small fields this matches well the trend shown in Fig. 5(c). Going beyond this crude approach and assuming harmonic-oscillator-type confinement [1,59], one gets Gaussian-like field BES dependence. This shape allows for very good fits to atomistic calculations [red dashed lines in Fig. 5(c)] with the BES not centered at zero field, again owing to alloying. For small fields, the Gaussian is consistent with a simple model, with the latter resembling the first terms of the Gaussian series expansion. QDs with smaller zero-field BES reach a threshold of 1 μeV [black dashed line in Fig. 5(c)] at smaller applied fields. The BES field reduction is associated with an increasing electron-hole spatial separation and thus decreasing BE oscillator strengths, with the oscillator strengths' evolution in field resembling that of the BES. For NWQDs considered in Fig. 5(c) there is approximately a fourfold reduction of the oscillator strength for BES reaching the 1 μeV threshold; thus, NWQDs with field-reduced BES remain optically active.

VI. SUMMARY

To summarize, it has been shown that alloying in NWQDs is responsible for the occurrence of nonvanishing BES merely owing to alloy randomness without any shape deformation, an off-center QD position, and nonuniform composition. The BES depends highly on the intermixing composition and varies considerably between individual dots. The splitting can be controlled by a vertical electric field; the field dependence is considerably different from that of SADs. The DE properties in NWQDs are also sensitive to the alloying. The DE gains notable optical activity that increases with alloying and quantum dot height. Heavily alloyed NWQDs can exhibit strongly out of plane polarized DE emissions, whereas in weakly alloyed NWQDs, the DE is polarized in plane.

ACKNOWLEDGMENTS

The author would like to thank Prof. D. Gershoni for discussions prior to this work. The support from the Polish National Science Centre based on Decision No. 2015/18/E/ST3/00583 is gratefully acknowledged.

[1] L. Jacak, P. Hawrylak, and A. Wojs, *Quantum Dots* (Springer, Berlin, 1998).

[2] *Single Semiconductor Quantum Dots*, edited by P. Michler, Topics in Applied Physics Vol. 90 (Springer, New York, 2003).

[3] D. Bimberg, M. Grundmann, and N. Ledentsov, *Quantum Dot Heterostructures* (Wiley, Chichester, UK, 1999).

[4] M. Bayer, G. Ortner, O. Stern, A. Kuther, A. A. Gorbunov, A. Forchel, P. Hawrylak, S. Fafard, K. Hinzer, T. L. Reinecke, S. N. Walck, J. P. Reithmaier, F. Klopf, and F. Schäfer, Phys. Rev. B **65**, 195315 (2002).

[5] P. Michler, A. Kiraz, C. Becher, W. V. Schoenfeld, P. M. Petroff, L. Zhang, E. Hu, and A. Imamoglu, Science **290**, 2282 (2000).

[6] C. Santori, M. Pelton, G. Solomon, Y. Dale, and Y. Yamamoto, Phys. Rev. Lett. **86**, 1502 (2001).

[7] R. M. Stevenson, R. J. Young, P. Atkinson, K. Cooper, D. A. Ritchie, and A. J. Shields, Nature (London) **439**, 179 (2006).

[8] E. Knill, R. Laflamme, and G. J. Milburn, Nature (London) **409**, 46 (2001).

[9] E. Waks, K. Inoue, C. Santori, D. Fattal, J. Vuckovic, G. S. Solomon, and Y. Yamamoto, Nature (London) **420**, 762 (2002).

[10] P. Kok, W. J. Munro, K. Nemoto, T. C. Ralph, J. P. Dowling, and G. J. Milburn, Rev. Mod. Phys. **79**, 135 (2007).

[11] R. Singh and G. Bester, Phys. Rev. Lett. **103**, 063601 (2009).

[12] M. Zieliński, Phys. Rev. B **88**, 115424 (2013).

[13] N. Akopian, G. Patriarche, L. Liu, J.-C. Harmand, and V. Zwiller, Nano Lett. **10**, 1198 (2010).

[14] M. Bouwes Bavinck, K. D. Jöns, M. Zieliński, G. Patriarche, J.-C. Harmand, N. Akopian, and V. Zwiller, Nano Lett. **16**, 1081 (2016).

[15] M. Zieliński, Y. Don, and D. Gershoni, Phys. Rev. B **91**, 085403 (2015).

[16] R. Singh and G. Bester, Phys. Rev. B **84**, 241402(R) (2011).

[17] R. Singh and G. Bester, Phys. Rev. Lett. **104**, 196803 (2010).

[18] M. Zieliński, K. Gołasa, M. R. Molas, M. Goryca, T. Kazimierczuk, T. Smoleński, A. Golnik, P. Kossacki, A. A. L. Nicolet, M. Potemski, Z. R. Wasilewski, and A. Babiński, Phys. Rev. B **91**, 085303 (2015).

[19] M. Zieliński, Phys. Rev. B **88**, 155319 (2013).

[20] O. Benson, C. Santori, M. Pelton, and Y. Yamamoto, Phys. Rev. Lett. **84**, 2513 (2000).

[21] M. Prilmüller, T. Huber, M. Müller, P. Michler, G. Weihs, and A. Predojević, Phys. Rev. Lett. **121**, 110503 (2018).

[22] I. Schwartz, D. Cogan, E. R. Schmidgall, L. Gantz, Y. Don, M. Zieliński, and D. Gershoni, Phys. Rev. B **92**, 201201(R) (2015).

[23] I. Schwartz, E. R. Schmidgall, L. Gantz, D. Cogan, E. Bordo, Y. Don, M. Zielinski, and D. Gershoni, Phys. Rev. X **5**, 011009 (2015).

[24] J. McFarlane, P. Dalgarno, B. Gerardot, R. Hadfield, R. Warburton, K. Karrai, A. Badolato, and P. Petroff, Appl. Phys. Lett. **94**, 093113 (2009).

[25] X. Xu, B. Sun, P. R. Berman, D. G. Steel, A. S. Bracker, D. Gammon, and L. Sham, Nat. Phys. **4**, 692 (2008).

[26] R. Ohta, H. Okamoto, T. Tawara, H. Gotoh, and H. Yamaguchi, Phys. Rev. Lett. **120**, 267401 (2018).

[27] C. Simon and J.-P. Poizat, Phys. Rev. Lett. **94**, 030502 (2005).

[28] G. Weihs, T. Huber, and A. Predojević, in *Quantum Dots for Quantum Information Technologies* (Springer, Cham, 2017), pp. 267–284.

[29] P. Michler (ed.), *Quantum Dots for Quantum Information Technologies*, Nano-Optics and Nanophotonics, Vol. 237 (Springer, Cham, 2017).

[30] G. Bester, S. Nair, and A. Zunger, Phys. Rev. B **67**, 161306(R) (2003).

[31] K. F. Karlsson, M. A. Dupertuis, D. Y. Oberli, E. Pelucchi, A. Rudra, P. O. Holtz, and E. Kapon, Phys. Rev. B **81**, 161307(R) (2010).

[32] M. A. Dupertuis, K. F. Karlsson, D. Y. Oberli, E. Pelucchi, A. Rudra, P. O. Holtz, and E. Kapon, Phys. Rev. Lett. **107**, 127403 (2011).

[33] R. J. Young, R. M. Stevenson, A. J. Shields, P. Atkinson, K. Cooper, D. A. Ritchie, K. M. Groom, A. I. Tartakovskii, and M. S. Skolnick, Phys. Rev. B **72**, 113305 (2005).

[34] W. Langbein, P. Borri, U. Woggon, V. Stavarache, D. Reuter, and A. D. Wieck, Phys. Rev. B **69**, 161301(R) (2004).

[35] N. Akopian, N. H. Lindner, E. Poem, Y. Berlatzky, J. Avron, D. Gershoni, B. D. Gerardot, and P. M. Petroff, Phys. Rev. Lett. **96**, 130501 (2006).

[36] K. Kowalik, O. Krebs, A. Lemaitre, S. Laurent, P. Senellart, P. Voisin, and J. Gaj, Appl. Phys. Lett. **86**, 041907 (2005).

[37] A. Bennett, M. Pooley, R. Stevenson, M. Ward, R. Patel, A. B. de La Giroday, N. Sköld, I. Farrer, C. Nicoll, D. Ritchie *et al.*, Nat. Phys. **6**, 947 (2010).

[38] R. M. Stevenson, R. J. Young, P. See, D. G. Gevaux, K. Cooper, P. Atkinson, I. Farrer, D. A. Ritchie, and A. J. Shields, Phys. Rev. B **73**, 033306 (2006).

[39] B. Gerardot, S. Seidl, P. Dalgarno, R. J. Warburton, D. Granados, J. Garcia, K. Kowalik, O. Krebs, K. Karrai, A. Badolato *et al.*, Appl. Phys. Lett. **90**, 041101 (2007).

[40] S. Seidl, M. Kroner, A. Högele, K. Karrai, R. J. Warburton, A. Badolato, and P. M. Petroff, Appl. Phys. Lett. **88**, 203113 (2006).

[41] J. D. Plumhof, V. Křápek, F. Ding, K. D. Jöns, R. Hafenbrak, P. Klenovský, A. Herklotz, K. Dörr, P. Michler, A. Rastelli, and O. G. Schmidt, Phys. Rev. B **83**, 121302(R) (2011).

[42] F. Ding, R. Singh, J. D. Plumhof, T. Zander, V. Křápek, Y. H. Chen, M. Benyoucef, V. Zwiller, K. Dörr, G. Bester, A. Rastelli, and O. G. Schmidt, Phys. Rev. Lett. **104**, 067405 (2010).

[43] J. Wang, M. Gong, G.-C. Guo, and L. He, Appl. Phys. Lett. **101**, 063114 (2012).

[44] R. Trotta, E. Zallo, C. Ortix, P. Atkinson, J. D. Plumhof, J. van den Brink, A. Rastelli, and O. G. Schmidt, Phys. Rev. Lett. **109**, 147401 (2012).

[45] R. Trotta, J. S. Wildmann, E. Zallo, O. G. Schmidt, and A. Rastelli, Nano Lett. **14**, 3439 (2014).

[46] A. Kors, J. P. Reithmaier, and M. Benyoucef, Appl. Phys. Lett. **112**, 172102 (2018).

[47] M. Abbarchi, T. Kuroda, T. Mano, and K. Sakoda, J. Phys.: Conf. Ser. **245**, 012049 (2010).

[48] M. T. Björk, C. Thelander, A. Hansen, L. Jensen, M. Larsson, L. R. Wallenberg, and L. Samuelson, Nano Lett. **4**, 1621 (2004).

[49] M. T. Borgström, V. Zwiller, E. Müller, and A. Imamoglu, Nano Lett. **5**, 1439 (2005).

[50] D. Dalacu, A. Kam, D. G. Austing, X. Wu, J. Lapointe, G. C. Aers, and P. J. Poole, Nanotechnology **20**, 395602 (2009).

[51] D. Dalacu, K. Mnaymneh, J. Lapointe, X. Wu, P. J. Poole, G. Bulgarini, V. Zwiller, and M. E. Reimer, Nano Lett. **12**, 5919 (2012).

[52] M. Bouwes Bavinck, M. Zieliński, B. J. Witek, T. Zehender, E. P. A. M. Bakkers, and V. Zwiller, Nano Lett. **12**, 6206 (2012).

[53] S. Yanase, H. Sasakura, S. Hara, and J. Motohisa, Jpn. J. Appl. Phys. **56**, 04CP04 (2017).

[54] M. A. M. Versteegh, M. E. Reimer, K. D. Jöns, D. Dalacu, P. J. Poole, A. Gulinatti, A. Giudice, and V. Zwiller, Nat. Commun. **5**, 5298 (2014).

[55] T. Huber, A. Predojevic, M. Khoshnegar, D. Dalacu, P. J. Poole, H. Majedi, and G. Weihs, Nano Lett. **14**, 7107 (2014).

[56] A. Tartakovskii, *Quantum Dots: Optics, Electron Transport and Future Applications* (Cambridge University Press, Cambridge, 2012).

[57] M. H. van Weert, N. Akopian, U. Perinetti, M. P. van Kouwen, R. E. Algra, M. A. Verheijen, E. P. Bakkers, L. P. Kouwenhoven, and V. Zwiller, Nano Lett. **9**, 1989 (2009).

[58] T. Takagahara, Phys. Rev. B **62**, 16840 (2000).

[59] E. Kadantsev and P. Hawrylak, Phys. Rev. B **81**, 045311 (2010).

[60] M. Korkusinski and P. Hawrylak, Phys. Rev. B **87**, 115310 (2013).

[61] P. N. Keating, Phys. Rev. **145**, 637 (1966).

[62] R. M. Martin, Phys. Rev. B **1**, 4005 (1970).

[63] C. Pryor, J. Kim, L. W. Wang, A. J. Williamson, and A. Zunger, J. Appl. Phys. **83**, 2548 (1998).

[64] T. Saito and Y. Arakawa, Phys. E (Amsterdam, Neth.) **15**, 169 (2002).

[65] J. C. Slater and G. F. Koster, Phys. Rev. **94**, 1498 (1954).

[66] J.-M. Jancu, R. Scholz, F. Beltram, and F. Bassani, Phys. Rev. B **57**, 6493 (1998).

[67] W. Jaskólski, M. Zieliński, G. W. Bryant, and J. Aizpurua, Phys. Rev. B **74**, 195339 (2006).

[68] M. Zieliński, Phys. Rev. B **86**, 115424 (2012).

[69] M. Zieliński, J. Phys.: Condens. Matter **25**, 465301 (2013).

[70] W. Sheng, S.-J. Cheng, and P. Hawrylak, Phys. Rev. B **71**, 035316 (2005).

[71] M. Zieliński, M. Korkusiński, and P. Hawrylak, Phys. Rev. B **81**, 085301 (2010).

[72] P. T. Różański and M. Zieliński, Phys. Rev. B **94**, 045440 (2016).

[73] P. T. Różański and M. Zieliński, Comput. Phys. Commun. **238**, 254 (2019).

[74] M. Świderski and M. Zieliński, Phys. Rev. B **95**, 125407 (2017).

[75] D. J. Chadi, Phys. Rev. B **16**, 790 (1977).

[76] S. Lee, F. Oyafuso, P. von Allmen, and G. Klimeck, Phys. Rev. B **69**, 045316 (2004).

[77] M. Zieliński, Acta Phys. Pol. A **122**, 312 (2012).

[78] E. Ivchenko, *Optical Spectroscopy of Semiconductor Nanostructures*, 2nd ed. (Alpha Science, Harrow, UK, 2005).

[79] L. He and A. Zunger, Phys. Rev. B **73**, 115324 (2006).

[80] G. W. Bryant, M. Zieliński, N. Malkova, J. Sims, W. Jaskólski, and J. Aizpurua, Phys. Rev. B **84**, 235412 (2011).

[81] V. Mlinar and A. Zunger, Phys. Rev. B **79**, 115416 (2009).

[82] T. Smoleński, T. Kazimierczuk, M. Goryca, T. Jakubczyk, Ł. Kłopotowski, Ł. Cywiński, P. Wojnar, A. Golnik, and P. Kossacki, Phys. Rev. B **86**, 241305(R) (2012).

[83] E. Poem, Y. Kodriano, C. Tradonsky, N. H. Lindner, B. D. Gerardot, P. M. Petroff, and D. Gershoni, Nat. Phys. **6**, 993 (2010).

[84] S. Marcet, K. Ohtani, and H. Ohno, Appl. Phys. Lett. **96**, 101117 (2010).

[85] Results of fitting using notation from Ref. [37] are for C_{2v} InAs/GaAs QD $s_0 = 0$ and $\gamma = 0.21\,\mu\text{eV}\,\text{kV}^{-1}/\text{cm}$ and for alloyed $\text{InGa}_{0.5}\text{As}_{0.5}$ $s_0 = 3.49\,\mu\text{eV}$ and $\gamma = 0.14\,\mu\text{eV}\,\text{kV}^{-1}/\text{cm}$.

[86] J. A. Barker and E. P. O'Reilly, Phys. Rev. B **61**, 13840 (2000).

[87] M. Zieliński, Nanoscale Res. Lett. **7**, 265 (2012).